Int J Adv Manuf Technol (2015) 79:1659–1670
DOI 10.1007/s00170-015-6941-5

ORIGINAL ARTICLE

Physics-based analysis of minimum quantity lubrication grinding

Yamin Shao · Beizhi Li · Kuo-Ning Chiang · Steven Y. Liang

Received: 10 October 2014 / Accepted: 20 February 2015 / Published online: 7 March 2015

Abstract Minimum quantity lubrication (MQL), which is to apply a minimum amount of lubricant directly into the contact zone, is a promising alternative to substantially reduce the lubricant cost caused by conventional flood cooling. In order to advance the MQL technique into grinding situations, understanding of the process and evaluation of the performance is necessary. Most documented studies thus far concerning MQL grinding are built upon experimental observations with individual and separate treatment of grinding performance measures such as grinding force, temperature, wheel wear, and surface roughness. This paper develops the analytical understanding of mechanical and thermal effects of MQL in grinding and profiles the MQL performance as functions of process and fluid application parameters. Physics-based predictive models are formulated to quantitatively describe the grinding force considering the lubrication effect of MQL. The friction coefficient under MQL condition is first predicted based on boundary lubrication theory, followed by the single grit force and grit distribution analysis. Further, surface roughness is calculated from the results of undeformed chip thickness distribution through probabilistic analysis. Additionally, energy partition and temperature distribution in the workpiece have been developed based on the moving heat source model. Material constitutive model are utilized to capture the influence of temperature and strain rate on the material flow stress. Experimental measurements of force, temperature, and surface roughness have also been pursued to calibrate and validate the predictive models.

Keywords MQL grinding · Mechanical-thermal coupled analysis · Single grit force · Energy partition · Surface roughness

Y. Shao (✉) · S. Y. Liang
George W. Woodruff School of Mechanical Engineering, Georgia Institute of Technology, 813 Ferst Dr. Rm. 211, Atlanta, GA 30332-0560, USA
e-mail: ymshao@gatech.edu

B. Li
College of Mechanical Engineering, Donghua University, 2999 North Renmin Rd., Songjiang District, Shanghai 201620, China

K.-N. Chiang
Department of Power Mechanical Engineering, National Tsing Hua University, 101 Section 2, Kuang-Fu Road, Hsinchu 30013, Taiwan

1 Introduction

Grinding is one of the major manufacturing processes which usually accounts for 20 to 25 % of the total expenditures on machining operations [1]. Grinding process requires very high energy input per unit volume of material removed, and virtually, all the energy is converted to heat. This leads to elevated temperatures in the grinding zone which can cause thermal damage to the workpiece and accelerated wheel wear. Grinding fluid is always used in industrial situations to diminish undesirable thermal effects by providing lubrication to reduce the amount of energy generated and directing cooling of the workpiece by convection [2].

However, economic and environmental drawbacks have been noticed for the conventional flood cooling method. The expense of cooling lubricant comprises nearly 20 % of the total manufacturing cost, and is several times higher than the tool costs [3]. Furthermore, grinding is often considered as the most environmentally unfriendly manufacturing process. The mist generation rate in grinding is often an order of magnitude higher than that in turning [4]. Researchers have been seeking for alternative cooling methods such as minimum quantity lubrication (MQL). MQL refers to the use of grinding fluids of only a minute amount, typically of a flow rate of 50 to 500 ml/h. This is about three to four orders of magnitude lower than the amount commonly used in flood cooling condition, where, for example, up to 10 l of fluid can be dispensed per minute [5]. In MQL grinding,

the lubricant fluid is mixed with pressurized air for delivery to the grinding zone for lubrication and cooling.

MQL has been successfully applied to various cutting processes such as turning, milling, and drilling, but MQL grinding is still a relatively new research area. Shen [6] studied the tribological properties and grinding performance of MQL grinding using nanofluids compared to pure water or oil MQL applications as well as dry and wet grinding. Nanofluids have shown benefits of reducing grinding forces, surface roughness, and wheel wear. Sadeghi et al. studied grinding force, surface roughness, and surface morphology behaviors under various process parameters and MQL fluid parameters in grinding of Ti-6Al-4V [7] and AISI 4140 steel [8]. Tawakoli et al. have conducted a series of experimental analysis of grinding force, surface roughness, surface morphology, grinding temperature, and energy partition in MQL grinding under different oil mist parameters [9], abrasive and coolant-lubricant types [10], and workpiece and grinding parameters [11]. Hadad et al. [12] have studied energy partition and temperature distribution in MQL grinding and demonstrated that the MQL grinding have provided some extent of cooling but not as efficient as wet grinding. While a considerable effort has been devoted to experimental investigations, literature shows very limited work in theoretical analysis of mechanical and thermal behavior in MQL grinding. Hadad and Sadeghi [13] have proposed an analytical model to calculate the temperature distribution in the workpiece under MQL grinding. Shao and Liang [14] proposed an approach to calculate the grinding force under MQL conditions from an analytical analysis of the single grit force and dynamic grit distribution. Most documented studies thus far concerning MQL grinding have focused on individual and separate treatment of grinding performance measures such as grinding force, temperature, wheel wear, and surface roughness.

In the interest of profiling the performance capability of MQL to support its broad-range process planning, this study presents the development of a realm of physics-based predictive models to quantitatively describe the mechanical and thermal effects of MQL in comparison to dry and flood cooling conditions in grinding. The predictions include grinding force, surface roughness, and workpiece temperature distribution. Boundary lubrication theory has been applied to describe the tribological behavior under MQL condition for calculation of the grinding forces. The surface roughness is modeled from the undeformed chip thickness distribution. The moving heat source model with a forced convectional heat loss is used to calculate the temperature distribution in the workpiece. To address the influence of high strain rate and temperature during the grinding process, the Johnson-Cook model is applied to capture the workpiece flow stress behavior. For calibration and validation purpose, experimental measurements of force, temperature, and surface roughness are taken during and after surface grinding of AISI 1018 workpiece material with aluminum oxide wheel (32A120KVBE). In summary, this work offers a comprehensive understanding of MQL grinding process and also acts as a tool for predicting and controlling the grinding performance based on input process parameters.

2 Force modeling

2.1 Friction coefficient prediction based on boundary lubrication theory

A prominent effect of the applied air-oil mixture in MQL grinding is lubrication, which changes the friction coefficient at the grit-workpiece interface. Due to the limited amount of lubricant, the lubricant film cannot be fully established. Therefore, the boundary lubrication theory is a more proper description of the MQL condition instead of hydrodynamic lubrication. In boundary lubrication, part of the load is carried by the metallic contacts between asperities on both surfaces and the other part is carried by adsorbed lubricant film contact. The friction force and the normal load in boundary lubrication can be expressed as

$$F = s_{\mathrm{m}} A_{\mathrm{m}} + s_{\mathrm{b}} A_b, \quad N = p_{\mathrm{m}} A_{\mathrm{m}} + p_{\mathrm{b}} A_{\mathrm{b}} \tag{1}$$

in which the metallic contact area A_{m} and the adsorbed lubricant film contact area A_{b} are calculated as follows according to the model presented by Kato et al. [15]:

$$\begin{aligned} A_{\mathrm{m}} &= \pi R\, n_0 D^2\, a_{\mathrm{s}}^3 / 6 H_{\max}^2, \\ A_{\mathrm{b}} &= \pi R n_0 D^2 \left[(a_{\mathrm{s}} + t_{\mathrm{b}})^3 - a_{\mathrm{s}}^3 \right] / 6 H_{\max}^2 \end{aligned} \tag{2}$$

in which R is the asperity tip radius, n_0 is the total asperity number given as $n_0 = A_0 z^2$, where A_0 is the apparent contact area, and z is the asperity density. D is the inclination distribution function, a_{s} is the approach of two surfaces, $H_{\max}$ is the asperity height distribution, and t_{b} is the effective adsorbed lubricant film thickness.

The friction coefficient is calculated from (1) as

$$\begin{aligned} \mu &= (s_{\mathrm{m}} A_{\mathrm{m}} + s_{\mathrm{b}} A_{\mathrm{b}}) / (p_{\mathrm{m}} A_{\mathrm{m}} + p_{\mathrm{b}} A_{\mathrm{b}}) \\ &= (C_1 A_{\mathrm{m}} + C_2 C_3 A_{\mathrm{b}}) / (A_{\mathrm{m}} + C_2 A_{\mathrm{b}}) \end{aligned} \tag{3}$$

where

$$C_1 = s_{\mathrm{m}} / p_{\mathrm{m}}, \quad C_2 = p_{\mathrm{b}} / p_{\mathrm{m}}, \quad C_3 = s_b / p_b, \tag{4}$$

where s_{b} and p_{b} and s_{m} and p_{m} are the shear strength and yield pressure at the adsorbed lubricant film contact area and the metallic contact area, respectively.

Substituting (2) into (1), the approach of two surfaces a_s can be estimated from the cubic function:

$$a_s^3 + 3C_2 t_b a_s^2 + 3C_2 t_b^2 a_s + \left[C_2 t_b^3 - N/(p_m Q)\right] = 0 \quad (5)$$

where

$$Q = \pi R n_0 D^2 / \left(6H_{max}^2\right) \quad (6)$$

From (2), (3), and (5), the friction coefficient between the grinding grit and workpiece can be calculated as

$$\mu = \frac{C_1 a_s^3 + C_2 C_3 \left\{(a_s + t_b)^3 - a_s^3\right\}}{a_s^3 + C_2\left[(a_s + t_b)^3 - a_s^3\right]} \quad (7)$$

The representative values for the parameters that have been used in boundary lubrication theory are given below in Sect. 5.

2.2 Single grit interaction model

Grinding is typically characterized by the multiple cutting points with large negative rake angle removing materials at very high strain rate. A stochastic treatment of the cutting edge geometry and distribution is necessary [16]. In this study, the grit shape is assumed to be conical with a rounded tip and a wear flat area. To describe the single grit interaction, a common three-stage assumption [1] is employed here. The single grit force is thus calculated from three components—chip formation, plowing, and rubbing force. The rubbing force and plowing force are dominant when the engagement depth of individual grit is very small. The chip formation only takes place when the undeformed chip thickness has reached a critical value [17]. Assuming that the single grit cutting process is orthogonal and treating the created chip as a series of elements with infinitesimal width, the individual grit grinding is simplified to a two-dimensional material removal process involving chip formation, plowing, and rubbing, as shown in Fig. 1.

Notice that all the rake angles here have negative values. The critical rake angle α_{cr} corresponds to the critical undeformed chip thickness t_{cr}. When undeformed chip thickness t is larger than t_{cr}, the material removal mechanism is chip formation. When t reaches t_{nom}, the rake angle will be equal to the nominal rake angle which is calculated from the grit cone angle. This microcutting mechanism can be represented by applying the Merchant model to each of the infinitesimal elements. The incremental chip formation force can be expressed as

$$\begin{aligned} dF_{tg,chip} &= \frac{\tau b \cos(\beta - \alpha)}{\sin\phi \cos(\phi + \beta - \alpha)} dt_1, \\ dF_{ng,chip} &= \frac{\tau b \sin(\beta - \alpha)}{\sin\phi \cos(\phi + \beta - \alpha)} dt_1 \end{aligned} \quad (8)$$

where τ is the workpiece material flow stress, b is the local cutting width, β is the friction angle, α is the local rake angle, and ϕ is the local shear angle. The local shear angle and local rake angle are related by cutting ratio rc.

$$\mathrm{rc} = \sin(\phi)/\cos(\phi - \alpha) \quad (9)$$

From geometrical relationship,

$$dt_1 = r\cos\alpha d\alpha \quad (10)$$

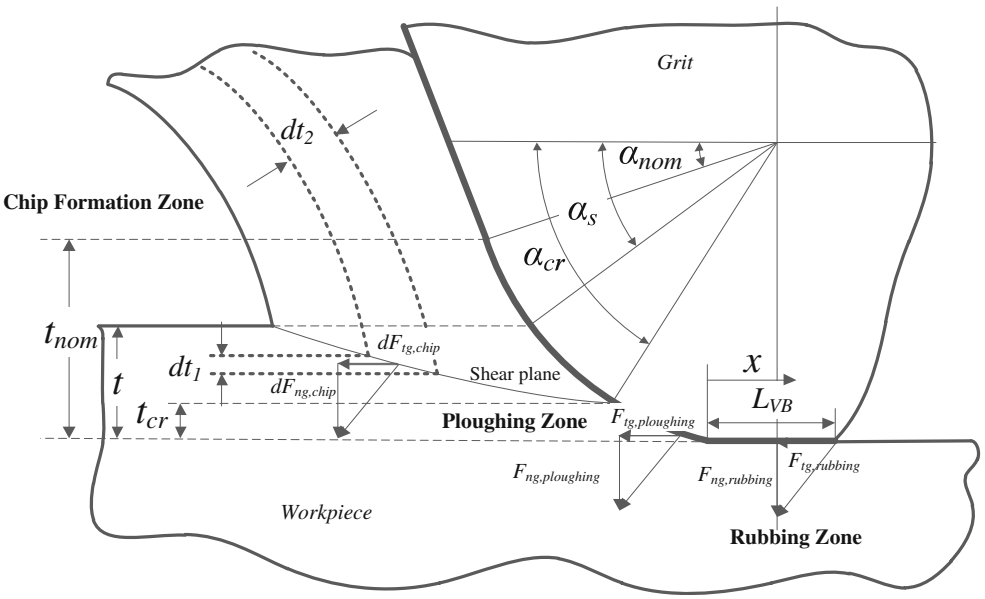

Fig 1 Single grit interaction illustration

The local width of cut for each individual grain is

$$\begin{aligned} b &= 2r\cos\alpha, \text{ if } t < t_{\text{nom}};\\ b &= 2(r\cos\alpha_{\text{nom}} + (t - t_{\text{nom}})/\tan(-\alpha)), \text{ if } t > t_{\text{nom}} \end{aligned} \tag{11}$$

By integration of the incremental tangential and normal forces per unit width in the two-dimensional simplified configuration, the chip formation force of each grit is calculated. The total tangential and normal force can thus be expressed as

When $t < t_{\text{nom}}$,

$$F_{\text{tg,chip}} = \int_{\alpha_{\text{cr}}}^{\alpha_s} \frac{\tau\cos(\beta-\alpha)}{\sin\phi\cos(\phi+\beta-\alpha)} 2r^2\cos^2\alpha d\alpha, \quad F_{\text{ng,chip}} = \int_{\alpha_{\text{cr}}}^{\alpha_s} \frac{\tau\sin(\beta-\alpha)}{\sin\phi\cos(\phi+\beta-\alpha)} 2r^2\cos^2\alpha d\alpha \tag{12}$$

When $t > t_{\text{nom}}$,

$$\begin{cases} F_{\text{tg,chip}} = \int_{\alpha_{\text{cr}}}^{\alpha_{\text{nom}}} \frac{\tau\cos(\beta-\alpha)}{\sin\phi\cos(\phi+\beta-\alpha)} 2r^2\cos^2\alpha d\alpha + \int_{t_{\text{nom}}}^{t} \frac{2\tau(r\cos\alpha_{\text{nom}} + (t-t_{\text{nom}})/\tan(-\alpha))\cos(\beta-\alpha_{\text{nom}})}{\sin\phi\cos(\phi+\beta-\alpha_{nom})} dt_1 \\ F_{\text{ng,chip}} = \int_{\alpha_{\text{cr}}}^{\alpha_{\text{nom}}} \frac{\tau\sin(\beta-\alpha)}{\sin\phi\cos(\phi+\beta-\alpha)} 2r^2\cos^2\alpha d\alpha + \int_{t_{\text{nom}}}^{t} \frac{2\tau(r\cos\alpha_{\text{nom}} + (t-t_{\text{nom}})/\tan(-\alpha))\sin(\beta-\alpha_{\text{nom}})}{\sin\phi\cos(\phi+\beta-\alpha_{\text{nom}})} dt_1 \end{cases} \tag{13}$$

The workpiece material below critical undeformed chip thickness is plastically deformed in front of the grit without chip formation. This phenomenon is referred to as the plowing effect. Shaw [18] adapted a Brinell indentation hardness test to describe this mechanism since the behavior of material beneath a Brinell ball resembles the material deformation below grit with a rounded tip. The Brinell hardness number, HB, is defined as the ratio of the load to the curved area of indentation:

$$\text{HB} = F_{\text{p}}/(\pi D t) \tag{14}$$

where F_{p} is the indentation force.

In the grinding process, the plastically deformed zone by the singe grit rotates in the direction of movement. Therefore, the plowing force can be calculated from the indentation force acting in the direction of half of the critical rake angle with respect to the normal direction. Additionally, a friction force between the grit and the workpiece is generated due to the relative movement. The tangential and normal plowing forces per grit can thus be estimated by considering the indentation effect and the friction reaction as

$$\begin{aligned} F_{\text{tg,ploughing}} &= F_{\text{p}}(\sin(\alpha_{\text{cr}}/2) + \mu\cos(\alpha_{\text{cr}}/2)),\\ F_{\text{ng,ploughing}} &= F_{\text{p}}(\cos(\alpha_{\text{cr}}/2) + \mu\sin(\alpha_{\text{cr}}/2)) \end{aligned} \tag{15}$$

The rubbing force is caused by the elastic or elastic-plastic contact of grit wear flat area with the workpiece surface [1]. Experimental investigations proved that the grinding force varies with different wear areas [19]. In most of the grinding force models [20–22], the rubbing forces are calculated from friction coefficient, contact pressure, and wear area. However, there models are based on the empirical relationship between average contact pressure and difference in radius of curvature [23]. This paper proposed an analytical approach to estimate the normal and shear stress in the wear flat area adapted from calculation of cutting force of worn tool [24]. The forces in the grinding direction $F_{\text{tg,rubbing}}$ and in the normal direction $F_{\text{ng,rubbing}}$ can

be calculated by integrating the normal stress and shear stress, respectively.

$$F_{\mathrm{tg,rubbing}} = b\int_0^{L_{\mathrm{VB}}} \sigma_{\mathrm{w}}(x)dx,$$
$$F_{\mathrm{ng,rubbing}} = b\int_0^{L_{\mathrm{VB}}} \tau_{\mathrm{w}}(x)dx \tag{16}$$

where

$$\begin{aligned}
&\sigma_{\mathrm{w}}(x) = \sigma_0((L_{\mathrm{VB}} - x)/L_{\mathrm{VB}})^2 \quad \text{for} \quad 0 < x < L_{\mathrm{VB}}\\
&\tau_{\mathrm{w}}(x) = \tau_0 \quad \text{for} \quad 0 < x < L_{\mathrm{VB}}\left(1 - \sqrt{\tau_0/\sigma_0}\right)\\
&\tau_{\mathrm{w}}(x) = \mu\sigma_{\mathrm{w}}(x) \quad \text{for} \quad L_{\mathrm{VB}}\left(1 - \sqrt{\tau_0/\sigma_0}\right) < x < L_{\mathrm{VB}}
\end{aligned} \tag{17}$$

where L_{VB} is the wear flat length as shown in Fig. 1. The flow stresses σ_0 and τ_0 are given in Waldorf's worn tool force model [25].

The total single grit forces in the tangential and normal directions are the summations of the forces due to chip formation, plowing, and rubbing, that is,

$$\begin{aligned}
F_{\mathrm{tg}} &= F_{\mathrm{tg,chip}} + F_{\mathrm{tg,ploughing}} + F_{\mathrm{tg,rubbing}},\\
F_{\mathrm{ng}} &= F_{\mathrm{ng,chip}} + F_{\mathrm{ng,ploughing}} + F_{\mathrm{ng,rubbing}}
\end{aligned} \tag{18}$$

An example of single grit force composition is shown in Fig. 2. When the undeformed chip thickness is very small (<1 μm), only plowing and rubbing forces contribute to the single grit force. After the critical undeformed chip thickness is reached, chip formation force increases rapidly and becomes the dominant factor at large undeformed chip thickness. Since not all the grits have the same engagement depth, the information of undeformed chip thickness distribution is necessary here to solve for the average single grit force.

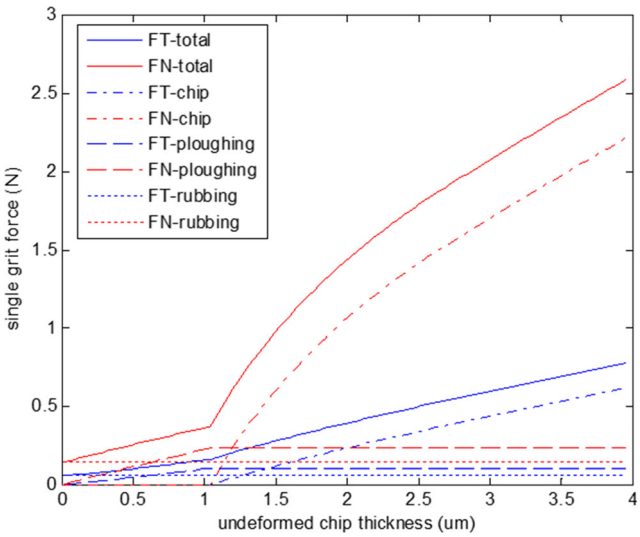

Fig 2 Single grit force composition

2.3 Distribution of undeformed chip thickness

Due to the randomness of grit distribution on the wheel surface, grits will have different engagement depths in the grinding process which result in different single grit forces. To calculate the average single grit force, it is necessary to know the distribution of undeformed chip thickness. This distribution was described by a Rayleigh probability density function (p.d.f.) [26].

$$f(t) = \begin{cases} \left(t/\sigma^2\right)\exp\left(-t^2/2\sigma^2\right) & t \geq 0\\ 0 & t < 0 \end{cases} \tag{19}$$

The expected value and variance is expressed as

$$\begin{aligned}
E(h) &= \sqrt{\pi/2}\sigma\\
\mathrm{sd}(h) &= \sqrt{0.429}\sigma
\end{aligned} \tag{20}$$

The parameter σ, that completely defined this p.d.f., was calculated as a function of the grinding wheel microstructure (grain shape, static grit density), dynamic effects (local grain deflection and wheel-workpiece contact deflection), and grinding conditions (wheel depth of cut, wheel and workpiece tangential velocity).

$$\sigma = \sqrt{aV_{\mathrm{w}}/(2V_{\mathrm{s}}l_{\mathrm{c}}C_{\mathrm{d}}\tan(\theta)) - t_{\mathrm{cr}}^2/2} \tag{21}$$

where a is the wheel depth of cut, V_{s} is the wheel speed, V_{w} is the workpiece speed, l_{c} is the real contact length due to wheel-workpiece contact deflection, and C_{d} is the dynamic grit density. The calculation details can be found in Hecker's work [27, 28].

Figure 3 shows a possible spectrum of undeformed chip thickness. The process parameters used in this example is shown in Table 1. Two regions of interest separated by the critical undeformed chip thickness t_{cr} can be observed, i.e., the rubbing and plowing region and the chip formation region. It is important to remark that what here is referred to as the undeformed chip thickness is actually the depth of engagement of each individual active grit regardless of whether it is plowing or removing material by chip formation. The Rayleigh distribution has the advantage of being uniquely defined by only one parameter σ.

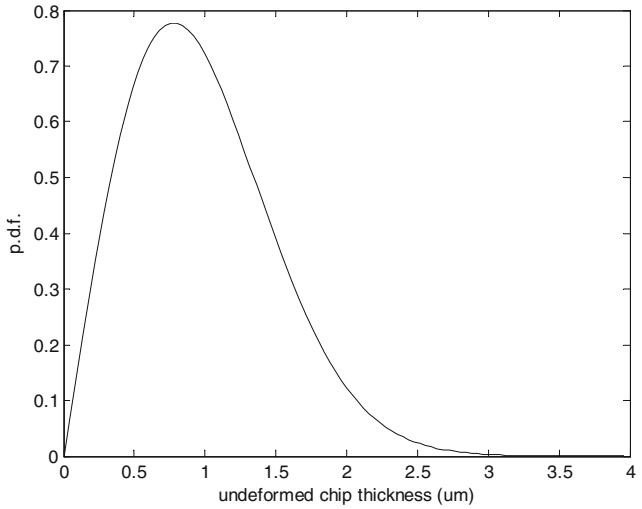

Fig 3 Undeformed chip thickness distribution

With the undeformed chip thickness distribution, the average single grit force or expectation of single grit force distribution are calculated by integration as given in (22). The total grinding forces are then calculated as multiplication of average single grit force and the number of active cutting edges in the contact zone.

$$\begin{cases} E\left(F_{\mathrm{tg}}\right) = \int_0^{\infty} f(t) F_{\mathrm{tg}}(t) dt \\ E\left(F_{\mathrm{ng}}\right) = \int_0^{\infty} f(t) F_{\mathrm{ng}}(t) dt \end{cases} \tag{22}$$

3 Surface roughness modeling

A typical parameter that has been used to quantify the quality of a surface topography is surface roughness. Many surface roughness models have been proposed based on wheel microstructure, kinematic conditions, surface generation simulations, and chip thickness analysis. An analytical model to predict the arithmetic mean surface roughness R_{a} directly from the estimated chip thickness probability density function is developed in [29]. A simple relation between the surface roughness and chip thickness was found. In MQL grinding, the surface generation mechanism is the same as in flood cooling conditions. Thus, the surface roughness in MQL grinding can be predicted from the undeformed chip thickness predictions in the same manner as in flood cooling condition.

Table 1 Process parameters used in undeformed chip thickness distribution example

Wheel speed (m/s)	Feed rate (m/min)	DOC (μm)	Lubrication
23.92	1.524	15.24	MQL

The arithmetic mean surface roughness can be defined as

$$R_{\mathrm{a}} = \frac{1}{L} \int_0^L |y - y_{\mathrm{CL}}| \, dl \tag{23}$$

where y_{CL} is the position of the centerline of the surface profile so that the area above and below the line are equal. The grooves generated by plowing or chip formation are assumed to be of the same characteristics and are described by the undeformed chip thickness. Assuming no overlap between the grooves and a triangular groove shape, the surface profile is represented in Fig. 4.

By definition, the areas below and above the centerline must be equal, given as

$$p' E\left(A'_{\mathrm{top}}\right) + p'' E(A'') = p' E(A'_{\mathrm{bottom}}) \tag{24}$$

where p' and p'' are the probabilities of a groove depth to be less and greater than y_{CL}, respectively, These probabilities can be mathematically described using undeformed chip thickness probability density function as

$$p' = \int_{y_{\mathrm{CL}}}^{\infty} f(t) dt \tag{25}$$

and

$$p'' = \int_0^{y_{\mathrm{CL}}} f(t) dt \tag{26}$$

By geometrical calculation of the groove areas and substitution of probability density function, the centerline position is calculated as

$$y_{\mathrm{CL}} = \sqrt{2/\pi}\,\sigma \tag{27}$$

Therefore, the total expected value for the surface roughness can be calculated as a weighted contribution as

$$E(R_{\mathrm{a}}) = p' E(R'_{\mathrm{a}}) + p'' E(R''_{\mathrm{a}}) \tag{28}$$

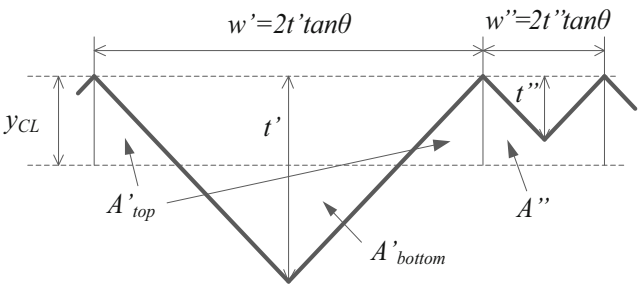

Fig 4 Theoretical surface profile generated by grooves

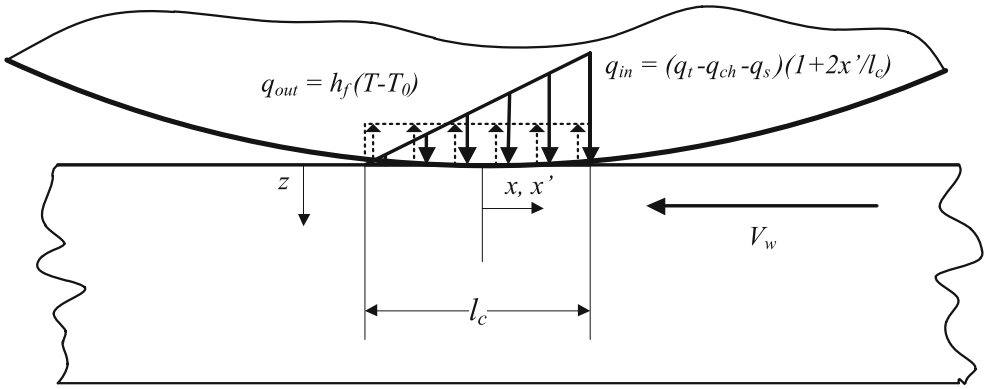

Fig 5 Temperature modeling schematic

The result of expected surface roughness can be mathematically calculated to be

$$E(R_a) = 0.37E(t) \tag{29}$$

However, a correction factor is necessary to adjust the empirical values to the analytical expression obtained in (29). The details of the calculation can be found in [29].

4 Temperature modeling

4.1 Temperature distribution in the workpiece

In this section, a complete thermal analysis of MQL effect in grinding process is developed. The moving heat source model based on Jaeger's work [30] is used to calculate the temperature distribution in the workpiece. Considering the heat input, there have been many discussions about the heat flux distribution. Early assumptions of a uniform heat distribution are not supported by temperature measurements. According to Rowe [31], triangular heat distribution should be used to avoid significant errors. In this work, a triangular heat source moving along the grinding direction and an additional uniform heat loss from MQL effect is modeled. The schematic diagram and coordinate system of temperature calculation are shown in Fig. 5.

Table 2 Thermal properties of AISI 1018 and Al_2O_3 wheel

Material	Thermal conductivity (W/m K)	Density (kg/m^3)	Specific heat (J/kg K)	Thermal diffusivity (m^2/s)
AISI 1018	51.9	7870	486	1.36e−5
Al_2O_3	46	3970	765	1.52e−5

The solution for the moving heat source can be represented by Bessel functions and obtained by summing over the length of the contact zone. The temperature at any point (x,z) in the workpiece is given as [31]

$$T_{(x,z)} = \int_{-l_c/2}^{l_c/2} (q_{in} - q_{out})/(\pi k_w)\exp(V_w(x-x')/(2\alpha_w)) \; K_0\left\{V_w\left[(x-x')^2 + z^2\right]^{1/2}/(2\alpha_w)\right\} dx' \tag{30}$$

where q_{in} is the total heat flux into the workpiece and fluid, q_{out} is the heat flux taken away by fluid, k_w is the thermal conductivity of the workpiece, and α_w is the thermal diffusivity given by $\alpha_w = k_w/\rho_w c_w$, where ρ_w is the workpiece density, c_w is the workpiece specific heat, and K_0 is the modified Bessel function of the second kind of order zero. The thermal properties of AISI 1018 and aluminum oxide wheel used in this study are listed in Table 2. The next step is to calculate q_{in} and q_{out} from energy partition analysis.

4.2 Energy partition in grinding process

In grinding process, the total heat in the contact zone flow into four heat sinks: the workpiece, the wheel, the chips and the fluid. That is,

$$q_t = q_w + q_s + q_{ch} + q_f \tag{31}$$

Table 3 Thermal properties of air and vegetable oil at room temperature

Material	Thermal conductivity (W/m K)	Density (kg/m^3)	Specific heat (J/kg K)	Dynamic viscosity (Pa s)
Air	0.026	1.16	1007	1.8e−5
Vegetable oil	0.17	980	1675	38.63e−3
Air-oil mixture	0.027	1.24	1035	1.92e−5

Table 4 Johnson-Cook parameters for AISI 1018 steel [35]

Material	A (MPa)	B (MPa)	n	C	m
AISI 1018	520	269	0.282	0.0476	0.553

The total heat flux is calculated from the grinding power as

$$q_t = F_t V_s/(w l_c) \tag{32}$$

where w is the grinding width. So, partition ratios can be defined as the proportions of these fluxes to the total flux. Based on the Hahn partitioning model for a grain sliding on a workpiece [32], a "workpiece-wheel" partition ratio, R_{ws} is defined as

$$R_{ws} = q_w/(q_w + q_s) = \left(1 + 0.97 k_g/\left(\sqrt{k_w \rho_w c_w}\sqrt{r_0 V_s}\right)\right)^{-1} \tag{33}$$

where k_g is the grain thermal conductivity and r_0 represents an effective radius of contact of the abrasive grains, here it is assumed to be equal to the grain tip radius. The ratio R_{ws} remains reasonably constant for a particular abrasive material and workpiece material, whereas the heat flux q_w entering the workpiece, taking account of the chips and fluid, is highly variable. Based on arguments by [1], the flux to the chips is assumed to be close to the limiting chip energy e_{ch}. For ferrous materials, this value is 6.21 J/mm^2. The flux convected by the chips is the rate of chip energy divided by the area of the grinding contact and is therefore

$$q_{ch} = e_{ch} a V_w / l_c \tag{34}$$

To estimate the heat flux entering the workpiece, the last step is the estimation of fluid convection. The heat flux taken by the MQL/fluid out of the contact zone is

$$q_f = h_f (T - T_0) \tag{35}$$

where h_f is the convection heat transfer coefficient of MQL/fluid, T_0 is the ambient temperature, and T is the workpiece temperature. For estimation of h_f in conventional flood cooling, Kim et al. [33] estimated values of 20,000 ahead and 15,000 W/m^2 K behind the grinding zone for downfeed creep grinding at relatively low temperatures. Rowe [31] estimated the values of 10,000 W/m^2 K for oil-in-water emulsion and 4000 W/m^2 K for neat oils. Hadad and Sadeghi [13] measured a value of 43,400 W/m^2 K for water-based coolants; for MQL fluid, a value of 1400 to 1630 W/m^2 K is obtained for different sets of MQL parameters. To analytically estimate the heat transfer coefficient, Hadad and Sadeghi [13] proposed a spraying cooling convection heat transfer model and considered the vaporization effect to estimate the heat transfer coefficient change from the trailing edge to the leading edge in MQL grinding. In this paper, the convection effect is considered as a fluid flow passing through parallel flat surfaces. The average heat transfer coefficient in the above equation can be estimated by the semiempirical model [34]:

$$\mathrm{Nu} = h_f l_c / k_f = 0.664 \mathrm{Pr}^{1/3} \mathrm{Re}^{1/2} \tag{36}$$

$$\mathrm{Pr} = \mu_f \mathrm{Cp}_f / k_f \tag{37}$$

$$\mathrm{Re} = u_f \rho_f l_c / \mu_f \tag{38}$$

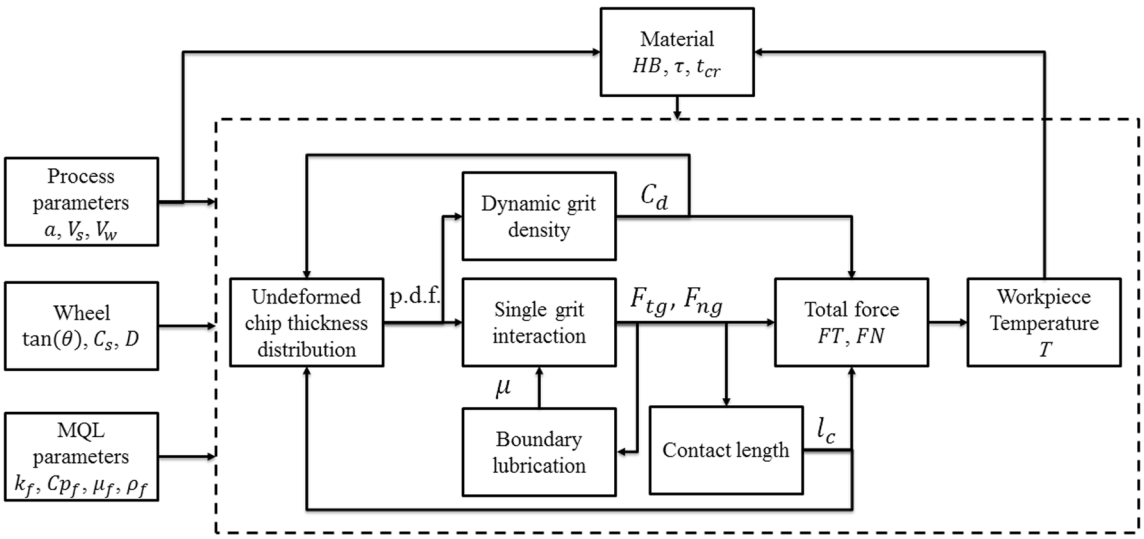

Fig 6 Overall algorithm for force and temperature calculation

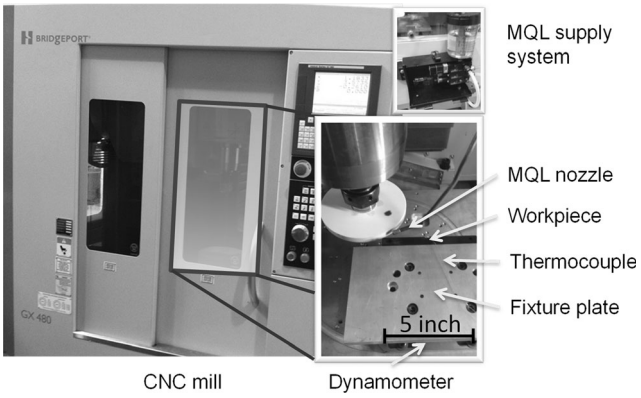

Fig 7 Experiment setup for surface grinding test

where Nu is the Nusselt number, Pr is the Prandtl number, and Re is the Reynolds number, k_f is the thermal conductivity, μ_f is the dynamic viscosity, Cp_f is the specific heat capacity, and ρ_f is the density of fluid. To estimate the MQL properties, a homogeneous two-phase flow is assumed here since the fluid drops have very high velocity and pressure [13]. In the homogeneous two-phase flow model, the air-oil mixture is considered as a single-phase flow with homogenous properties. A heat loss with heat transfer coefficient h_f is modeled to capture the heat taken out by the MQL fluid. The thermal properties of air and vegetable oil as well as the calculated thermal properties for air-oil mixture used in the experiment are listed in Table 3.

4.3 Material constitutive model

To incorporate strain, strain rate, and temperature influences, the Johnson-Cook model is applied to calculate the flow stress on the shear plane in the grinding process.

$$\sigma = (A + B\varepsilon^n)\left(1 + C\ln\left(\frac{\dot{\varepsilon}}{\dot{\varepsilon}_0}\right)\right)\left(1 - \left[\frac{(T - T_r)}{(T_m - T_r)}\right]^m\right) \quad (39)$$

Strain and strain rate calculation for grinding process are given in [21]. For the AISI 1018 material used in the experiment, the Johnson-Cook parameters are given in Table 4.

Table 5 Process parameters and lubrication conditions

Lubrication	MQL			Wet		
Condition no.	1	2	3	1	2	3
Depth of cut (μm)	15.24	15.24	7.62	15.24	15.24	7.62
Feed rate (m/min)	1.524	0.762	1.524	1.524	0.762	1.524
Wheel speed (m/s)	23.92	23.92	23.92	23.92	23.92	23.92
Specific material removal rate (mm^2/s)	0.387	0.194	0.194	0.387	0.194	0.194

Table 6 Parameters in boundary lubrication calculation

Parameter	t_b	C_2	C_3	H_{max} (μm)	R (μm)	D	z
Representative value	0.2	0.5	0.5	10	20	1.5	20

The temperature effect to the flow stress is incorporated in an iterative manner since the force calculation will influence the energy input for the temperature.

To summarize, the overall algorithm for the force and temperature modeling is shown in Fig. 6. C_d, μ, and l_c are calculated in the iterative calculation of undeformed chip thickness distribution and single grit force. The coupling effect of force and temperature is also realized in an iterative manner through the application of J-C material constitutive model.

5 Experimental validation

To validate the force and temperature predictions, a series of experiments with different process parameters and lubrication conditions have been performed on the Bridgeport GX480 Vertical Milling Center. The CNC milling center was used instead of the grinding machine for the following reasons: (1) simple setup of the measurement equipment, (2) precise control of spindle rotational speed up to 10,000 RPM, and (3) a high positional accuracy of 0.00254 mm. The MQL system is manufactured by UNIST, Inc. with the lubrication medium of vegetable oil and flow rate constant at 396 ml/h, and the air pressure was kept at 4 bars. The distance between the nozzle and the grinding zone is 40 mm and the impingement angle is 10°. The workpiece is AISI 1018 steel rectangular bar with a width of 9.5 mm. The grinding wheel used for the experiments was Norton 38A120-KVBE aluminum oxide friable wheels with a diameter of 150 mm. The wheel was dressed by Norton single point diamond dresser with 16 μm of dressing depth and overlap ratio of 1.68. The grinding force components were recorded using a piezoelectric transducer-based dynamometer (type Kistler 9257B). Temperature was recorded using Omega type K thermocouple (5TC-TT-K-36-36) and Omega OM-DAQ-USB-2401 Data Acquisition System with a sampling frequency of 100 Hz. The hot junction of the thermocouple was welded by thermal epoxy to the bottom of a blind hole with 1.5 mm distance to the ground surface. The workpiece roughness was measured by Zygo white light

Table 7 Single grit force and dynamic grit density calculation

Lubrication	MQL		
Condition no.	1	2	3
$E(F_{tg})$ (N)	0.177	0.130	0.144
$E(F_{ng})$ (N)	0.603	0.348	0.418
C_d ($1/mm^2$)	2.4	2.1	1.9

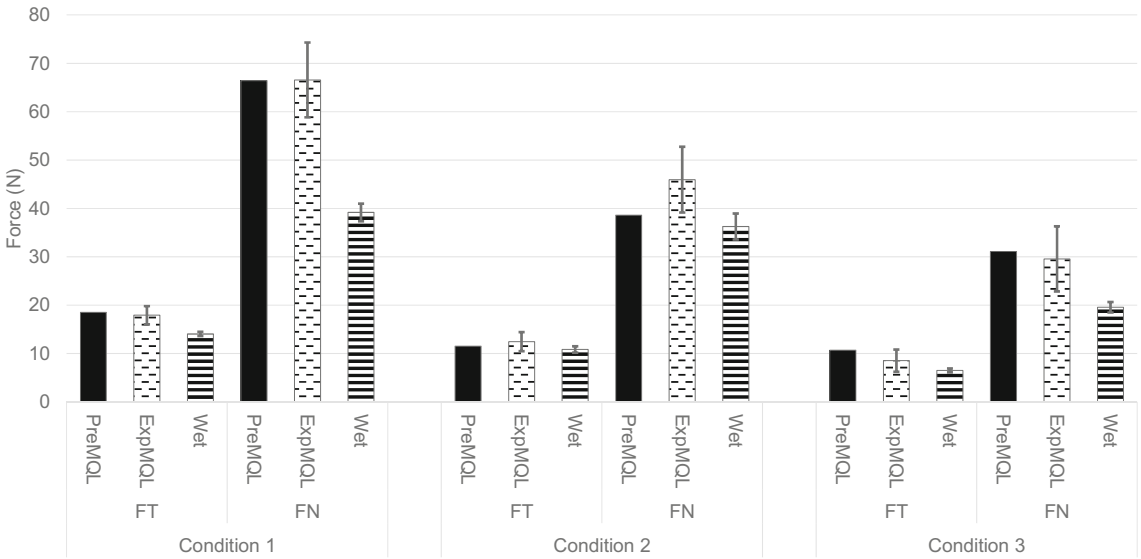

Fig 8 Comparison between predicted and experimental force results

interferometer. The surface roughness measurement result is taken as the average of three different points of ground surface. The experiment setup is shown in Fig. 7.

In order to compare the effects of lubrication type on MQL performances, six sets are divided into two groups: MQL and conventional flood cooling (represented as "wet" condition). For each group, three different process conditions have been performed. Since the chip removal in MQL grinding is not as efficient as in flood cooling, some prior experiments have been performed to ensure no chip accumulation or clogging in MQL grinding occurs. The process parameters and lubrication conditions are summarized in Table 5.

The coefficients used in friction coefficient calculation under boundary lubrication conditions are summarized in Table 6. The parameter C_1 is calibrated to be 0.2 under MQL condition.

The friction coefficient calculations are then used in the single grit force calculation. The average single grit force and the dynamic grit density calculated in three conditions are listed in Table 7. It is observed that the average single grit force and dynamic grit density are significantly higher in condition 1 where the material removal rate is two times as in condition 2 or 3. The total force is calculated as a production of single grit force in (22) and the total number of dynamically cutting grit in the contact area.

The force comparison for tangential and normal grinding forces is shown in Fig. 8. Condition 1 is used to calibrate the C_1 in boundary lubrication and wear flat length L_{VB}. In each cluster, the first column represents the predicted force in MQL grinding, the second column represents the experimental force in MQL grinding, and the third column represents the experimental force in flood cooling condition.

As it can be seen, the tangential grinding force under MQL condition is slightly higher than that in flood cooling condition. In MQL grinding, due to the limited amount of fluid, the lubricant film cannot be fully established, which will lead to a higher local friction coefficient and thus higher plowing force component as well as friction force component. Another reason is that the capability of chip removal in MQL grinding is not ideal as in flood cooling. The remaining chips on the wheel surface may cause some extra friction. However, although the amount of fluids was reduced by about a thousand times, MQL grinding still achieved similar performance as flood cooling. This is due to efficient penetration of oil mist to the grinding zone that provides certain lubrication.

Table 8 Surface roughness comparison

Process condition	Condition 1		Condition 2		Condition 3	
Lubrication	MQL	Wet	MQL	Wet	MQL	Wet
Average undeformed chip thickness (μm)	0.73	0.69	0.57	0.54	0.62	0.59
Average predicted surface roughness (μm)	0.22	0.15	0.15	0.12	0.19	0.15
Average measured surface roughness (μm)	0.22	0.20	0.17	0.16	0.19	0.17

The simulated data shows a good agreement with the experimental data in both tangential and normal directions. The average error of predictions is 13.67 %. The possible error source could come from environment influence or the uncounted factors from wheel topography or workpiece conditions.

The surface roughness across the grinding direction for each condition is presented in Table 8. It is observed that MQL has similar surface finish as flood cooling condition. As mentioned before, the surface generation mechanism in MQL grinding is the same as in flood cooling conditions. Thus, the surface roughness in MQL grinding can be predicted from the undeformed chip thickness predictions in the same manner as in flood cooling condition. The change of friction coefficient in MQL grinding slightly increased the average undeformed chip thickness which results in a slightly higher surface roughness. The experimental measurements of surface roughness shows good consistence with the model predictions.

In order to estimate the convection heat transfer coefficient of air-oil mixture h_f, the Nusselt number, Prandtl number, and Reynolds number in three conditions are calculated and summarized in Table 9. The estimated heat transfer coefficient is also shown in Table 9. It should be mentioned that in the literature, it is common to assume that the coolant velocity through the grinding zone is equal to the peripheral wheel speed. For high-velocity air-oil mist used in MQL, it is acceptable to make an assumption that air-oil mist velocity can be approximated by taking the average of oil mist velocity in the MQL nozzle exit and the wheel speed. It is noticed that the heat transfer coefficients are fairly small comparing to the flood cooling conditions with a typical value of around 40,000 W/(m^2 K) [1].

Table 10 shows the comparison of maximum temperature rise at 1.5 mm depth and the energy partition ratio between experimental and simulation. The predictions in flood cooling condition are calculated based on the assumption of convection heat transfer coefficient of 40,000 W/(m^2 K).

From the results, it is indicated that the proposed analytical model is able to estimate the energy partition and temperature rise in MQL grinding. The experimental results suggested that the model slightly underestimate the convection heat transfer by the air-oil mist. The possible reason could be that the simulation did not take into account of the cooling effect on the side of the workpiece or outside the grinding zone. It is very obvious that the predicted energy partition in the flood cooling conditions are much higher than experimental results since the side cooling effect in flood cooling conditions are very strong due to the extensive amount of coolant.

Table 9 Estimation of heat transfer coefficient h_f

Process condition	Condition 1	Condition 2	Condition 3
Lubrication	MQL	MQL	MQL
Reynolds number	2.45e4	2.59e4	2.52e4
Prandtl number	0.7245	0.7245	0.7245
Nusselt number	93.26	96.05	94.66
Estimated h_f (W/(m^2 K))	779	757	768

Table 10 Comparison between predicted and measured max temperature rise

Process condition	Condition 1		Condition 2		Condition 3	
Lubrication	MQL	Wet	MQL	Wet	MQL	Wet
Predicted energy partition ratio to the workpiece	0.85	0.39	0.85	0.39	0.83	0.38
Measured energy partition ratio to the workpiece	0.77	0.2	0.74	0.2	0.72	0.15
Predicted maximum t emperature rise (K)	112	32	104	27	52	20
Measured maximum temperature rise (K)	103	16	90	14	44	8

6 Conclusions

The physics-based predictive models for MQL grinding have been developed to quantitatively profile the process performance in the context of grinding force, temperature, and surface roughness. The modeling approach is based on cutting mechanics, kinematics, and heat transfer analysis. In this study, convoluted relationships between different process performance like friction coefficient, force, undeformed chip thickness distribution, and temperature take place. The friction coefficient in boundary lubrication is governed by the force developed between the wheel and the workpiece and the contact geometry. Further, the undeformed chip thickness and dynamic grit density are indirectly influenced by the single grit force. In the meanwhile, the single grit force is determined by the undeformed chip thickness and friction coefficient. Also, the temperature calculation based on the force input and the calculated temperature will directly influence the material flow stress behavior and thus influence the grinding force calculation. The iterative procedure is employed during the simulation process and it is shown to be stable and various conditions. Surface grinding of AISI 1018 workpiece with aluminum oxide wheel under various process parameters were pursued, and the predicted grinding forces, temperature, and surface roughness were compared to experimental measurements, and reasonable agreements in the context of magnitudes and trends were found.

It is found that the application of MQL can effectively lubricate the grit-workpiece interface and produce similar tangential grinding force as compared to flood cooling conditions. However, MQL is expected to generate much more heat during

grinding as a result of limited amount of coolant been applied. Therefore, it is much easier for MQL grinding to reach critical temperature that may trigger thermal damage and burn. This heating issue could be diminished by using CBN wheel with better thermal conductivity. It is still suggested for MQL grinding to perform non-aggressive process conditions if no external cooling assistance was employed. Finally, the capability profiling results from this study can support further MQL process planning and optimization on quantitative scales.

References

1. Malkin S (1989) Grinding technology: theory and applications of machining with abrasives. Ellis Howard Ltd., Prentice Hall
2. Guo C, Malkin S (1992) Analysis of fluid flow through the grinding zone. J Eng Ind 114(4):427–434
3. Klocke F, Eisenblatter G (1997) Dry cutting. CIRP Ann 46(2):519–526
4. Chen Z, Yamaguchi H, Liang S (2002) Predictive modeling of cutting fluid aerosol in grinding process. Trans NAMRI/SME 277–285
5. Autret R, Liang S (2003) Minimum quantity lubrication in finish hard turning. Proceedings of International Conference on Humanoid, Nano Technology, Information Technology, Communication and Control, Environment, and Management
6. Shen B (2008) Minimum quantity lubrication grinding using nanofluids. Dissertation, University of Michigan
7. Sadeghi M, Hadad M, Tawakoli T, Emami M (2009) Minimal quantity lubrication—MQL in grinding of Ti-6Al-4V titanium alloy. Int J Adv Manuf Technol 44:487–500
8. Sadeghi M, Hadad M, Tawakoli T, Emami M (2010) An investigation on surface grinding of AISI 4041 hardened steel using minimum quantity lubrication-MQL technique. Int J Mater Form 3:241–251
9. Tawakoli T, Hadad M, Sadeghi M (2010) Influence of oil mist parameters on minimum quantity lubrication—MQL grinding process. Int J Mach Tools Manuf 50(6):521–531
10. Tawakoli T, Hadad M, Sadeghi M (2010) Investigation on minimum quantity lubricant-MQL grinding of 100Cr6 hardened steel using different abrasive and coolant-lubricant types. Int J Mach Tools Manuf 50(8):698–708
11. Tawakoli T, Hadad M, Sadeghi M, Daneshi A, Stockert S, Rasifard A (2009) An experimental investigation of the effects of workpiece and grinding parameters on minimum quantity lubrication—MQL grinding. Int J Mach Tools Manuf 49(12–13):924–932
12. Hadad M, Tawakoli T, Sadeghi M, Sadeghi B (2012) Temperature and energy partition in minimum quantity lubrication-MQL grinding process. Int J Mach Tools Manuf 54–55:10–17
13. Hadad M, Sadeghi B (2012) Thermal analysis of minimum quantity lubrication-MQL grinding process. Int J Mach Tools Manuf 63:1–15
14. Shao Y, Liang S (2014) Predictive force modeling in MQL (minimum quantity lubrication) grinding. Proceedings of the ASME 2014 Manufacturing Science and Engineering Conference, Michigan
15. Kato S, Marui E, Hashimoto M (1998) Fundamental study on normal load dependency of friction characteristics in boundary lubrication. Tribol Trans 41(3):341–349
16. Hecker R (2002) Part surface roughness modeling and process optimal control of cylindrical grinding. Dissertation, Georgia Institute of Technology
17. Son S, Lim H, Ahn J (2005) Effects of the friction coefficient on the minimum cutting thickness in micro cutting. Int J Mach Tools Manuf 45(4–5):529–535
18. Shaw M (1996) Principles of abrasive processing. Oxford University Press
19. Li L, Fu J (1980) A study of grinding force mathematical model. CIRP Ann 29:245–259
20. Malkin S, Cook N (1971) The wear of grinding wheels, part 1, attritious wear. J Manuf Sci Eng 93(4):1120–1128
21. Tang J, Du J, Chen Y (2009) Modeling and experimental study of grinding forces in surface grinding. J Mater Process Technol 209: 2847–2854
22. Durgumahanti U, Singh V, Rao P (2010) A new model for grinding force prediction and analysis. Int J Mach Tools Manuf 50:231–240
23. Kannappan S, Malkin S (1972) Effect of grain size and operating parameters on the mechanics of grinding. J Manuf Sci Eng 94(3): 833–842
24. Li K, Liang S (2007) Modeling of cutting forces in near dry machining under tool wear effect. Int J Mach Tools Manuf 47:1292–1301
25. Waldorf DJ, DeVor RE, Kapoor S (1998) A slip-line field for ploughing during orthogonal cutting. J Manuf Sci Eng 120(4):693–699
26. Younis M, Alawi H (1984) Probabilistic analysis of the surface grinding process. Trans CSME 8(4):208–213
27. Hecker R, Liang S, Wu X, Xia P, Guo W (2007) Grinding force and power modeling based on chip thickness analysis. Int J Adv Manuf Technol 33(5–6):449–459
28. Hecker R, Ramoneda I, Liang S (2003) Analysis of wheel topography and grit force for grinding process modeling. J Manuf Process 5(1):13–23
29. Hecker R, Liang S (2003) Predictive modeling of surface roughness in grinding. Int J Mach Tools Manuf 43(8):755–761
30. Jaeger J (1942) Moving sources of heat and the temperature at sliding contacts. J Royal Soc NSW 84(21):4316–4318
31. Rowe W (2001) Thermal analysis of high efficiency deep grinding. Int J Mach Tools Manuf 41:1–19
32. Hahn R (1962) On the nature of the grinding process. Proceedings of the 3rd MTDR Conference
33. Kim N, Guo C, Malkin S (1997) Heat flux distribution and energy partition in creep-feed grinding. CIRP Ann 46(1):227–232
34. Bergman T, Lavine A, Incropera F, Dewitt D (2011) Fundamentals of heat and mass transfer. 7th ed. John Wiley & Sons, Inc
35. List G, Stter G, Bouthiche A (2012) Cutting temperature prediction in high speed machining by numerical modelling of chip formation and its dependence with crater wear. Int J Mach Tools Manuf 54–55:1–9